Neuron
Article

Rapid Axonal Sprouting and Pruning Accompany Functional Reorganization in Primary Visual Cortex

Homare Yamahachi,[1] Sally A. Marik,[1] Justin N.J. McManus,[1] Winfried Denk,[2] and Charles D. Gilbert[1,*]
[1]The Rockefeller University, New York, NY 10065, USA
[2]Max Planck Institute for Medical Research, Heidelberg, Germany
*Correspondence: gilbert@rockefeller.edu
DOI 10.1016/j.neuron.2009.11.026

SUMMARY

The functional architecture of adult cerebral cortex retains a capacity for experience-dependent change. This is seen following focal binocular lesions, which induce rapid changes in receptive field size and position. To follow the dynamics of the circuitry underlying these changes, we imaged the intrinsic long-range horizontal connections within the lesion projection zone (LPZ) in adult macaque primary visual cortex. To image the same axons over time, we combined viral vector-mediated EGFP transfer and two-photon microscopy. The lesion triggered, within the first week, an ~2-fold outgrowth of axons toward the center of the LPZ. Over the subsequent month, axonal density declined due to a parallel process of pruning and sprouting but maintained a net increase relative to prelesion levels. The rate of turnover of axonal boutons also increased. The axonal restructuring recapitulates the pattern of exuberance and pruning seen in early development and correlates well with the functional changes following retinal lesions.

INTRODUCTION

The cerebral cortex retains the capacity for experience-dependent changes throughout life. Experience-dependent plasticity in the adult primary visual cortex (V1) occurs during perceptual learning (Crist et al., 2001; Li et al., 2004, 2006; Schoups et al., 2001) or following altered sensory input resulting from CNS damage (Baker et al., 2005; Calford et al., 2000; Chino et al., 1995; Darian-Smith and Gilbert, 1994, 1995; Das and Gilbert, 1995; Giannikopoulos and Eysel, 2006; Gilbert et al., 1990; Heinen and Skavenski, 1991; Kaas et al., 1990; Keck et al., 2008; Mataga et al., 2004; Rose et al., 1960). When a circumscribed part of V1 is functionally deafferented by focal binocular retinal lesions, this area, known as the lesion projection zone (LPZ), is initially unresponsive to visual stimuli but over time regains visually driven activity (Chino et al., 1992; Darian-Smith and Gilbert, 1995; Das and Gilbert, 1995; Gilbert and Wiesel, 1992). Some of these changes occur rapidly. Within hours following the lesion, the receptive fields (RFs) of the neurons inside the LPZ shift to parts of the retina surrounding the lesion (which we will refer to as the peri-LPZ). Over time, the recovery of visually driven activity and the associated remapping of visual topography progress toward the center of the LPZ. The circuit underlying the reorganization is likely to involve the intrinsic long-range horizontal connections formed by the axons of cortical pyramidal cells. The extent of these connections matches the area of reorganization (Gilbert and Wiesel, 1979), and following the lesion they undergo sprouting and synaptogenesis (Darian-Smith and Gilbert, 1994). Axonal sprouting could explain the recovery of visually driven activity of neurons inside the LPZ and the remapping of cortical topography occurring months after the lesion. The earlier studies were based on postmortem tracing of connections and comparisons of horizontal projections to the LPZ and to normal cortex ~1 year postlesion. Now two-photon microscopy allows us to perform longitudinal studies of identified processes in the intact, living brain. The additional advantage of this approach is that it enables us to follow rapid changes in cortical circuitry associated with the short-term changes in RFs and topography.

Two-photon microscopy has permitted the imaging of individual retinotectal axons (Ruthazer et al., 2006) and cortical axons during development (Portera-Cailliau et al., 2005), as well as in the adult brain (De Paola et al., 2006; Majewska et al., 2006; Stettler et al., 2006) for extended periods of time. In the absence of any disruption of sensory input, boutons appear and disappear at a rate of 7% per week, while axonal density remains stable (Stettler et al., 2006). This observation was based on labeling of the axons by the delivery of genetically encoded fluorophores with viral vectors. With one such vector, AAV, we were able to induce long-term, stable expression of the transgene in specific cortical neurons. Here, we combined two-photon imaging of the enhanced green fluorescent protein (EGFP) delivered with these viral vectors to perform a longitudinal analysis of axon dynamics in V1 during the functional reorganization following retinal lesions.

RESULTS

To study the changes in cortical circuitry associated with retinal lesions, we combined electrophysiological mapping, labeling of the long-range horizontal connections with viral vectors, and two-photon microscopy in macaque primary visual cortex. The horizontal connections are formed by layer 2/3 cortical pyramidal neurons and run for long distances parallel to the cortical surface (on the order of 8 mm). Because of their considerable length, they link neurons with widely separated RFs (Stettler et al., 2002) and are therefore good candidates for providing input from neurons with RFs outside the retinal lesion to neurons within the LPZ.

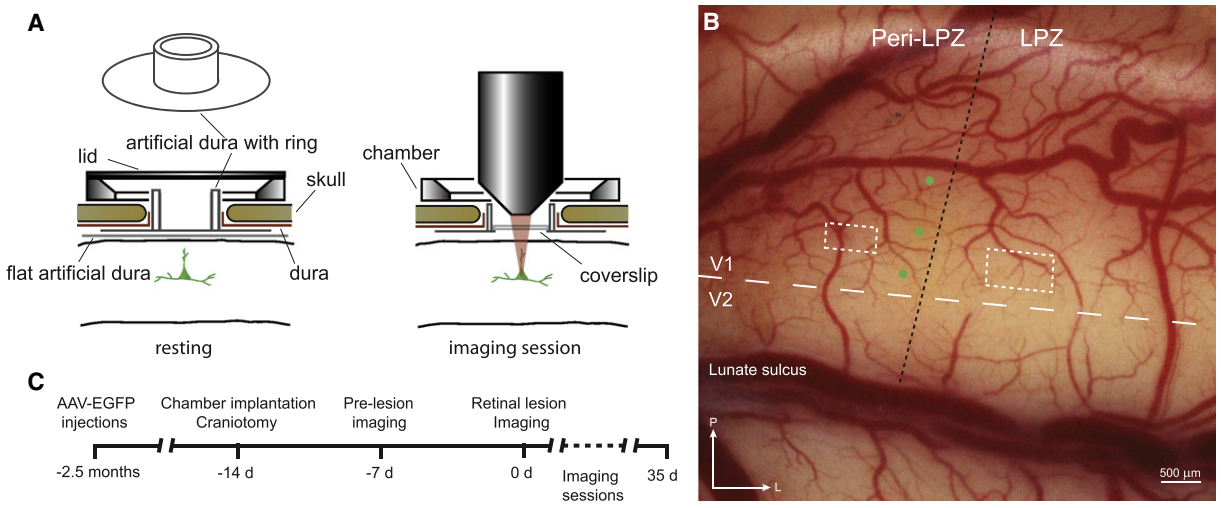

Figure 1. Experimental Protocol

(A) Custom-built imaging chamber for long-term chronic in vivo imaging of axonal segments.

(B) Diagram showing the AAV-EGFP injections into V1 (green dots). The dashed rectangles indicate the areas imaged in the LPZ and the Peri-LPZ. The black dashed line indicates the border of the LPZ.

(C) Timeline of the experimental protocol.

The two-photon imaging technique (Denk et al., 1990) allowed us to do the necessary longitudinal studies, i.e., follow the same axons over time. We used a preparation for chronic imaging of neuronal structure in vivo (Stettler et al., 2006) (Figure 1A), which involved injecting a genetically engineered, nonreplicative adeno-associated virus (AAV) carrying the EGFP gene under the control of a CMV promoter. We made a series of injections of the virus into V1 along an antero-posterior axis, perpendicular to the V1/V2 border (Figure 1B). EGFP expression was achieved in most of the neurons in an ~0.5 mm radius around the injection site. We then waited for a period of at least 2 months for full expression of the transgene in the infected neurons. This achieves a steady state of expression and complete labeling of neurons and their processes (Reimsnider et al., 2007; Stettler et al., 2006), so that any changes observed from that point are not due to alterations in levels of expression of the transgene. To prepare for imaging, we made a craniotomy over the opercular surface of V1 and inserted an artificial dura. This provided a window for imaging and inhibited regrowth of the dura over the imaged area (see Experimental procedures). Two areas of cortex were imaged, one medial and one lateral, ~1 mm from the injection sites. One of the imaged regions was within the planned LPZ and the other within the surrounding peri-LPZ (Figure 1B). It is important to note that all the axons imaged, in both regions, originated from the same group of fluorescently labeled neurons. For each of the imaged regions, we collected 9–20 Z stacks, covering a total volume of 0.10–0.22 mm^3. Each stack contained 100 images, with a 250 μm field of view, that spanned 200 μm in depth. On the day of making the retinal lesions, we first mapped the topography of the V1 area under the craniotomy with extracellular recordings. This map provided the guide for making the lesions, which were placed so that their boundaries lay to the lateral side of the virus injections, such that the infected neurons were located within the peri-LZP, ~1 mm outside the LPZ. The lesions were placed at corresponding locations on the two retinas, so the LPZ would be completely devoid of retinal input immediately following the lesion (Figure 1B). This allowed us to study axonal projections both into the LPZ and the peri-LPZ.

Axonal Dynamics in the LPZ following Binocular Retinal Lesions

Labeled axons within the LPZ and peri-LPZ were imaged several times spanning a period of 7–8 weeks (see Figure 1C for timeline). For comparison between time points, we selected areas that provided clear images over the entire period. Axons were reconstructed using a semi-automatic tracing program (Neuromantic, www.rdg.ac.uk/neuromantic) to make 3D reconstructions of all the axons in the imaged areas. When comparing changes between regions, we reconstructed axons over the same cortical depths. To detect any appearance or disappearance of axon collaterals and boutons from week to week, we compared the same areas imaged at different time points. The same procedure was done for two animals, both of which showed similar changes. The first and most dramatic change was an increase in axon density immediately after the lesion. In the first animal (MA) changes were seen on the day of the lesion (imaged 4:30 to 9 hr after making the lesions), with an increase in density by a factor of 2.8 relative to 1 week prior to the lesion (−7 days versus 0.25 days, Figures 2A, 3A, and 3B, $p < 1 \times 10^{-5}$, bootstrapping test). The second animal (MB) also showed the initial exuberant increase in axon density, first measured 7 days after the lesion (Figures 2B, 3D, and 3E, $p = 0.002$, bootstrapping test). The addition of axons (Figures 3A and 3D, yellow fibers) was more pronounced toward the center of the LPZ where the baseline density was quite sparse. Another striking feature of the response to the lesion was a process of axonal pruning that accompanied the sprouting. In MA, this is seen at the 14 days postlesion time point, where relative to the axons imaged

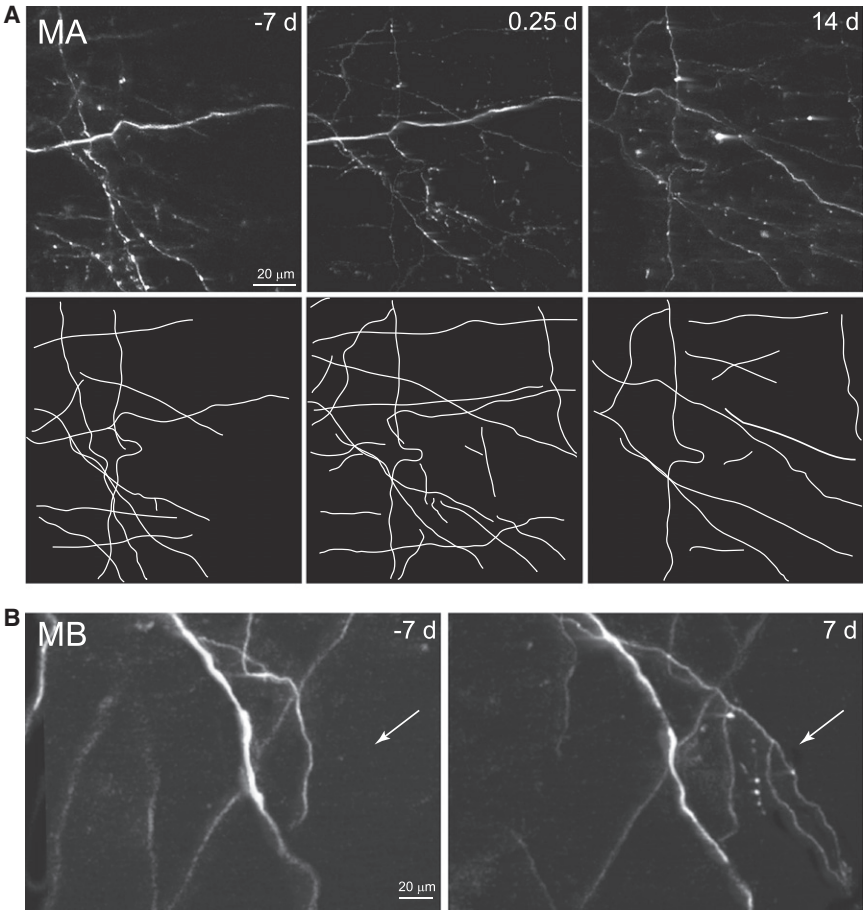

Figure 2. LPZ Imaged at 7 Days before, after, and 14 Days after the Lesion

(A) (Upper panel) A projection of Z stacks to a depth of 150 μm shows axonal segments in MA. (Lower panel) Reconstructions of axonal segments traced through the Z stacks. Note how axon density increased markedly from the day of the lesion (imaged 4:30 to 9 hr postlesion) onward (0.25 days to 14 days). Streaking in the images is due to photomultiplier saturation. These images are a subset of the tracings shown in Figure 5.

(B) The appearance of a new axonal segment is shown at 7 days (arrow) in the second monkey (MB).

on the day of the lesion, 46.1% were pruned and 37.5% were added. In MB, elimination matches addition at 21 days (59.5% versus 58.5%), while at 35 days the axons being eliminated are more numerous than those being added (65.0% versus 31.8%). The overall density, however, remained elevated even at 28 days after the lesion in MA (194%, $p = 0.003$; bootstrapping test), while in MB at 35 days, the remaining increase in net density after the pruning was not statistically significant (119%, $p = 0.47$; bootstrapping test). There were minor differences between both animals—for example, in MB a higher fraction (46.8% compared to 24.8%, Figures 3C and 3F) of axons present before the lesion was still present after 35 days (28 days in MA). In both animals, though, new axons that appeared at any time point were much more likely to be lost at the subsequent time point than "stable" axons that were present before the lesion or for at least two consecutive time points. Over all the axons in the LPZ from both monkeys, 84% of the axons that appeared at any time point were lost before the subsequent imaging session, while only 48% of "stable" axons were lost over the same time period ($p < 1 \times 10^{-10}$; two-sided two-proportion z test).

Axons displayed several distinct elimination behaviors (Figures 4A and 4B). One example is an axon that existed at the time of the lesion and then, at 14 days postlesion, showed degenerative changes, including beading, swelling, retraction of short side branches, and detachment of axon fragments from their parent shaft (Figure 4A). By 28 days, this axon collateral had disappeared completely. Another axon present before the lesion showed a progressive retraction of the axonal tip (Figure 4B).

Comparison of Axonal Dynamics in the LPZ with a Baseline Control

The vigorous axonal sprouting we observed in the LPZ contrasts sharply with the relative stability of axonal density in the nondeprived cortex. A previous study by Stettler et al. (2006), which was carried out using the same apparatus and imaging protocol used here, established the extent of boutonal and axonal density dynamics in the normal, nondeprived macaque V1. We used the raw data from that study as a control, in order to compare the axonal dynamics in the LPZ with the dynamics in the normal cortex. To this end, we reanalyzed a subset of data taken from the control study (Stettler et al., 2006) consisting of two Z stacks that were clearly imaged at both time points. These stacks were chosen only on the basis of the imaging quality, rather than on the dynamical attributes of the axons or boutons. From the current dataset, we used the entire reconstructed cortical volume, from the two time points in each monkey that most nearly coincided with the time points used in the Stettler et al. (2006) study. We then compared the distribution of axonal changes obtained from the control data with the distribution from our new lesion data, using a nonparametric statistical test (the Brunner-Munzel test; see Experimental procedures). We found that the net changes in axonal length in the Stettler et al. (2006) study were significantly less than the changes we observed in lesioned monkeys ($p = 3.8 \times 10^{-5}$; one-sided Brunner-Munzel test). As an alternative approach, we performed a resampling test, to compute the probability that the sprouting of any random sample of LPZ axons is less than the axonal changes in the control data. This probability ($p = 4.5 \times 10^{-5}$) closely matches the p value computed from the Brunner-Munzel test. These results demonstrate that the axonal sprouting we observed in the LPZ was not an artifact of our imaging procedures and that

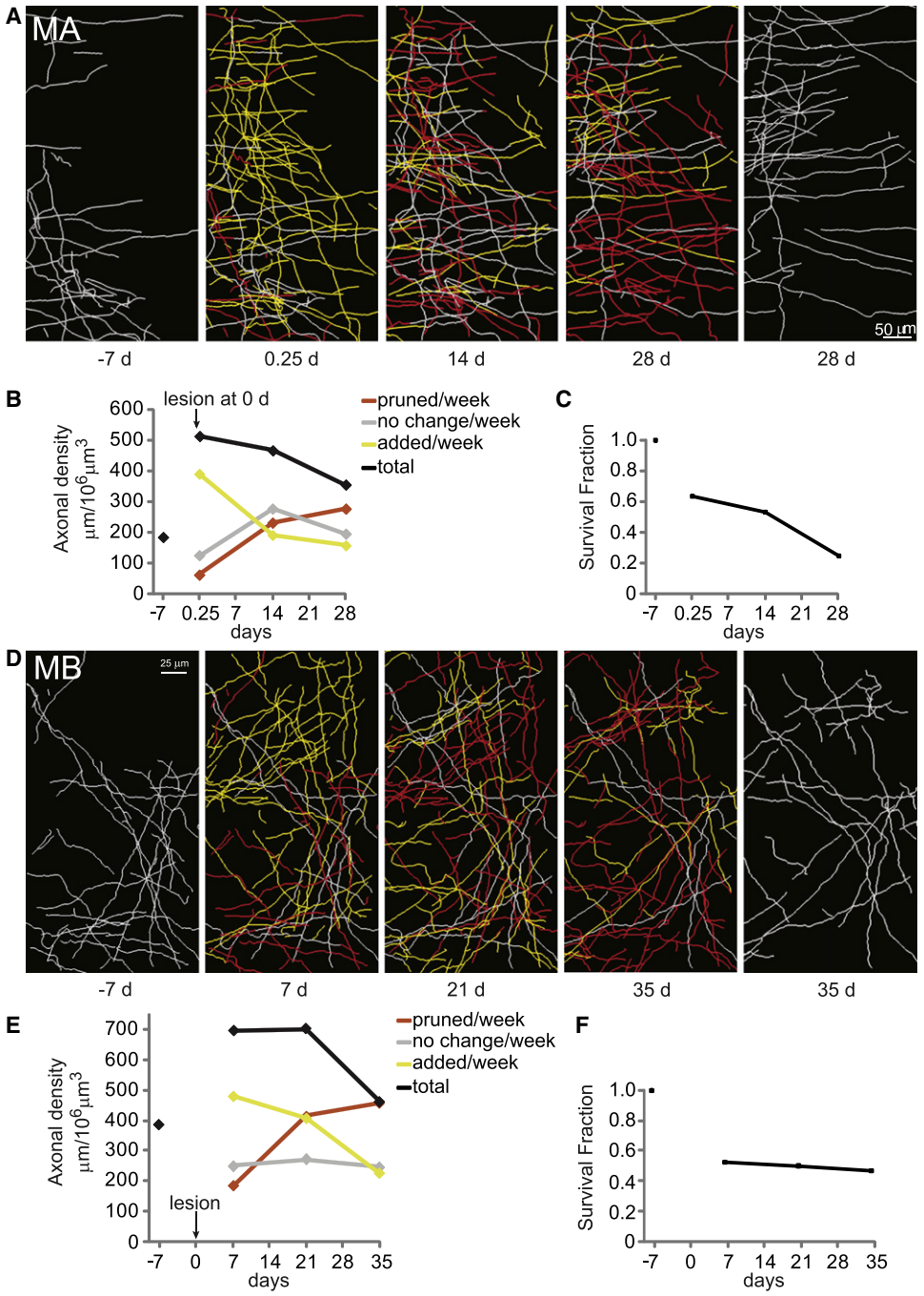

Figure 3. Axonal Dynamics in LPZ

(A) Axonal tracing of Z stacks acquired through a depth of 200 µm. Gray, axon segments that remained unchanged compared to the previous time point; yellow, segments that were added; red, segments eliminated. Last panel shows the axons present at the end of the imaging session.

(B) Axon density (axonal length per unit of volume) for axons that had been added (yellow), pruned (red), and remained unchanged (gray) since the preceding imaging section. The total axonal density is shown in black.

(C) Axonal survival fraction. Axonal length still present from the initial axonal population (−7 days) as a fraction of the total initial length.

(D–F) Figure description exactly as above.

our control data set from Stettler et al. (2006) is sufficiently large to distinguish the net axonal changes in the LPZ from those in the normal cortex.

Axonal Boutons

In addition to the strikingly rapid turnover of axon branches, we also observed a turnover of axonal boutons (on axons that

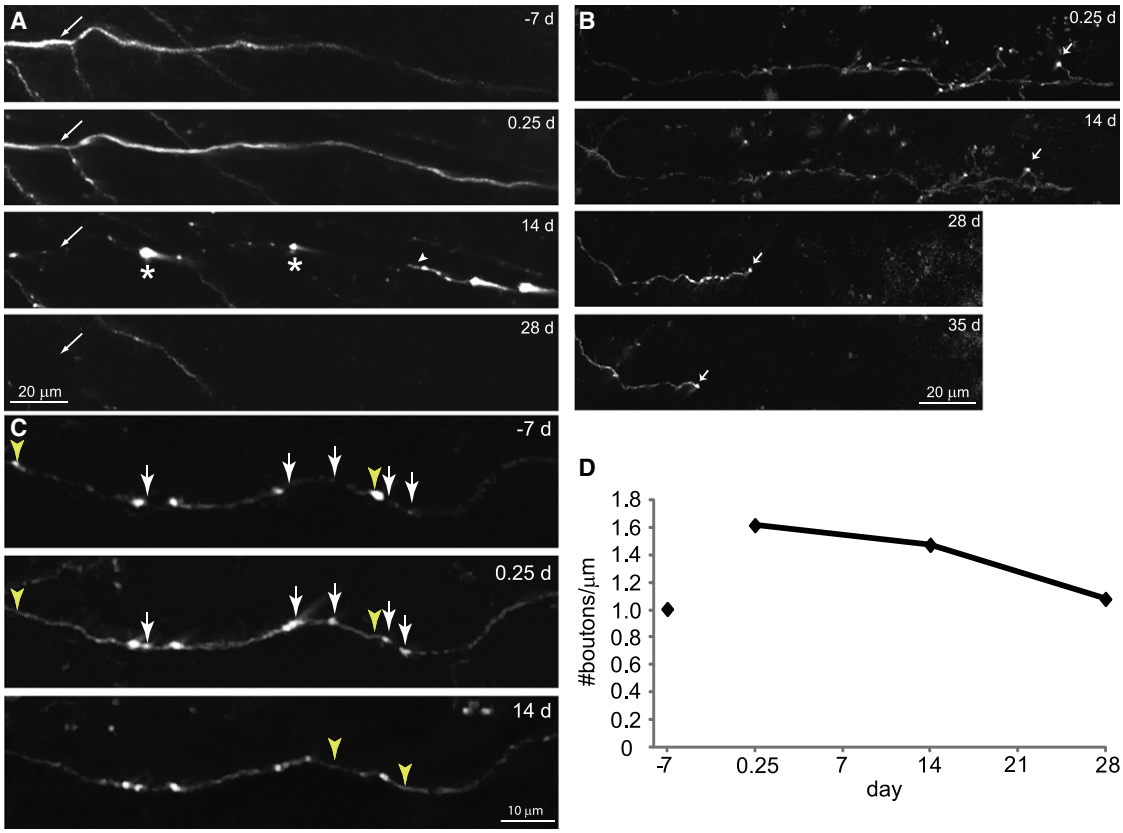

Figure 4. Axon Pruning Modes and Bouton Turnover in LPZ

(A) An axon branch previously shown in Figure 2 (arrow) present before (−7 days) and after the lesion (0.25 day, imaged 4:30 to 9 hr postlesion) undergoes degeneration by 14 days. Note the beading and swelling (*) and detachment of portions of axonal shaft (arrowhead). By 28 days, remnants of the segment were no longer detected.

(B) Retraction of a terminal branch (arrow) is shown in a segment from 0.25–35 days.

(C) An axon segment showing an increase in bouton density immediately after the lesion (four white arrows) and two being eliminated (yellow arrowheads).

(D) Bouton density.

were retained) that was significantly higher (peak rates of 72% and 32%, for appearance and disappearance, respectively, during the week between −7 days and 0.25 days, for 17 axon segments totaling 1.24 mm in length, Figures 4C and 4D) than the baseline turnover rate (in nondeprived animals, Stettler et al., 2006) of ~7% per week. During the last 2 weeks of our observation period, more boutons were eliminated than added (48.9% versus 15.6%), resulting in a return of the bouton density to the level seen prior to the lesion.

Axonal Changes in the Peri-LPZ

The axonal projections from the injection sites into the peri-LPZ not only showed a pattern of changes that was different from that seen inside the LPZ but also different from those in nondeprived animals. After a retinal lesion, even in the peri-LPZ, axon addition and elimination were more active than in the nondeprived animal. For instance, in the peri-LPZ from MA, 58% of the axons that were present at the first imaging session (−7 days) disappeared before the next time point (7 days); and 48% of the axons that were present at the second time point (7 days) appeared sometime after the first imaging session (−7 days). These rates of axonal retraction and addition were significantly higher than the rates observed in the control data that we reanalyzed from the Stettler et al. (2006) study (retraction: $p = 0.0011$; addition: $p = 0.031$; one-sided two-proportion z test). In MA, although there was an elevation in both axonal sprouting and pruning, the rate of pruning, over the whole imaging period, was somewhat higher than the rate of addition (44% versus 27%), and consequently there was a net reduction of 16.5% in axon density after the lesion (Figure 5A). In the other animal, MB, following the lesions, the rates of sprouting and pruning were roughly in balance, so that there was no change in overall axon density over the time period of observation (Figures 5B and 5C).

Both within the LPZ and peri-LPZ, therefore, retinal lesions triggered an immediate massive and highly dynamic program of axonal sprouting and pruning. In the LPZ, the axon density increased, while in the peri-LPZ, the density dropped or remained constant.

DISCUSSION

After retinal lesions, beginning on the same day, the plexus of long-range horizontal axons shows remarkable changes consistent with the alterations in RF position and size. Just as the RF changes begin

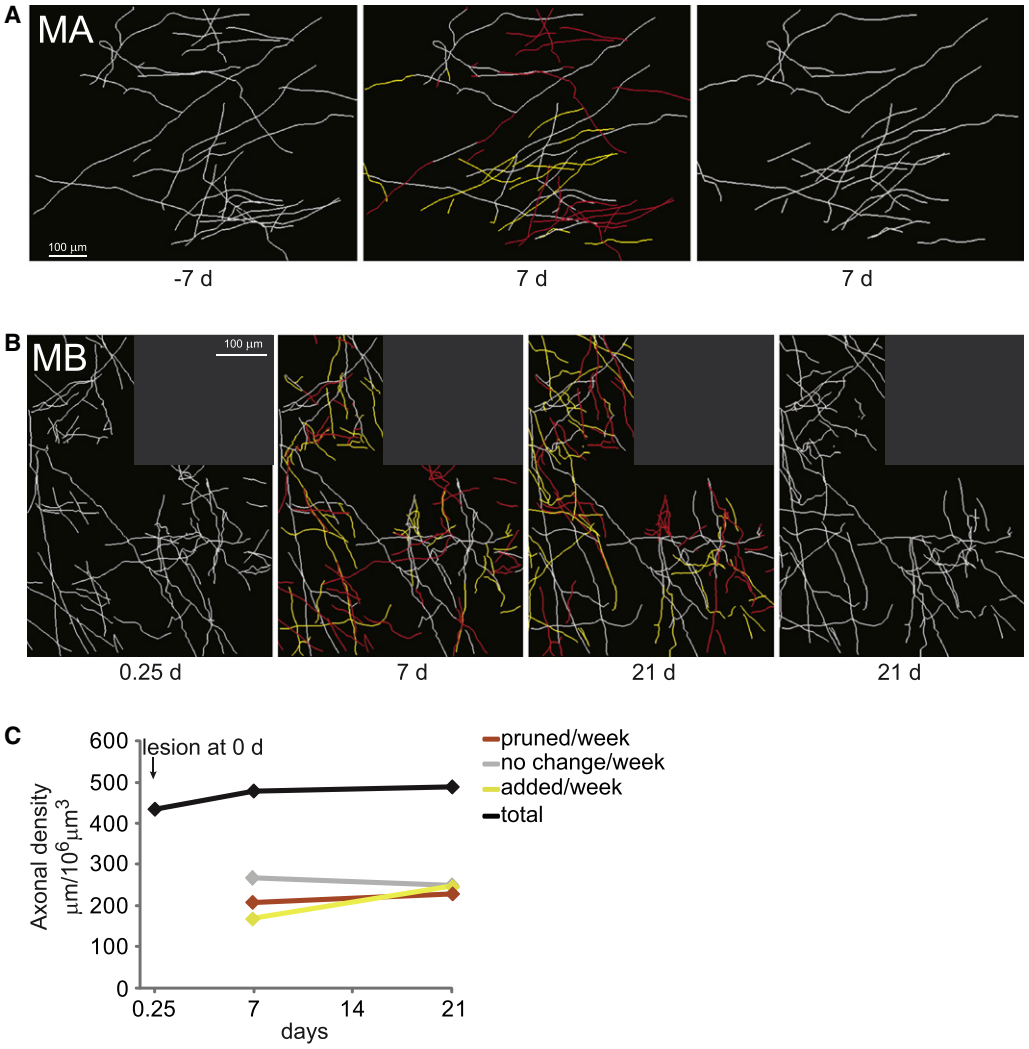

Figure 5. Axonal Dynamics in Peri-LPZ (MA and MB)

(A) Axonal tracing of Z stacks from MA acquired through a depth of 100 µm. Axon segments that remained unchanged since the previous time point are shown in gray; segments that were added are in yellow; those eliminated in red.

(B) MB, description as in (A).

(C) Axon density represented as axonal length per unit of volume from MB. Axon addition (yellow) and elimination (red) occurred at similar rates, resulting in a stable overall axon density (black).

immediately after the lesion is made, axon collaterals sprout and synaptic boutons proliferate from the outset of the lesion. Following the lesion, RFs are initially much larger than those seen in normal visual cortex, but over time contract to their normal size, although with shifted RF centers (Darian-Smith and Gilbert, 1995; Gilbert and Wiesel, 1992). Similarly, horizontal axons proliferate at the highest rate during the days following the lesion. Their density within the LPZ reaches a peak in the first week, then drops, somewhat, due to an accelerated rate of axonal pruning, but can remain elevated for at least as long as the observation period of 7–8 weeks.

Axonal Sprouting following Retinal Lesions

In the absence of retinal lesions, the density of horizontal axonal arbors is stable, but boutons are quite dynamic (De Paola et al., 2006; Stettler et al., 2006). This baseline of structural dynamics may be what allows substantial morphological changes to begin immediately following alterations of visual experience. The model of focal binocular retinal lesions provides a window into the structural basis of experience-dependent cortical plasticity. Initially, the cortical region representing the area of the damaged retina is silenced, but over a period of minutes to months, it recovers visually driven activity (Baker et al., 2005; Calford et al., 2000; Chino et al., 1995; Darian-Smith and Gilbert, 1994, 1995; Das and Gilbert, 1995; Giannikopoulos and Eysel, 2006; Gilbert et al., 1990; Gilbert and Wiesel, 1992; Heinen and Skavenski, 1991; Kaas et al., 1990; Keck et al., 2008; Palagina et al., 2009). Though one fMRI study comes to a different conclusion (Smirnakis et al., 2005), fMRI may not provide an accurate determination of the LPZ boundary (see Calford et al., 2005 for a further discussion of the issues involved). The other studies

cited above found extensive cortical remapping, on the basis of electrophysiology, optical imaging and fMRI, following retinal lesions. The lack of reorganization at the level of projections from the lateral geniculate nucleus or the thalamus suggests that the topographic reorganization in V1 is due to changes in intracortical connectivity (Darian-Smith and Gilbert, 1995). Postmortem analysis of cortical connections 8 months after the removal of sensory input showed that axonal sprouting of long-range horizontal connections made by pyramidal neurons in V1 accompanies functional reorganization in adult striate cortex (Darian-Smith and Gilbert, 1994). Furthermore, the pattern of orientation columns before the lesion and after recovery is conserved, which supports the role of the plexus of horizontal connections in the topographic reorganization (Das and Gilbert, 1995). Further evidence, that strengthening of lateral connectivity is involved in the recovery following retinal lesions, is provided by voltage-sensitive dyes recordings in the adult rat visual cortex (Palagina et al., 2009). This indicates that intercolumnar connections mediated by long-range horizontal axons, which under normal conditions play a modulatory role (Hirsch and Gilbert, 1991), develop a suprathreshold influence following recovery, leading to the shift in RF position for neurons in the LPZ. Moreover, a recent theoretical model demonstrates that the functional and perceptual recovery following retinal lesions may be explained by this strengthening of lateral connectivity in V1 (McManus et al., 2008).

While axonal sprouting over weeks and months provided a comfortable explanation for the long-term changes in cortical topography occurring months after the lesion, the question remained as to how the rapid changes seen as early as on the day of the lesion could occur. One might have supposed that the fast shift in RFs is due to an increase in the effectiveness of existing synapses. In the adult mouse visual cortex, dendritic spines show a 3-fold increase in turnover starting 2 days after retinal lesions and lasting for 2 months (Keck et al., 2008). In the current study, we show that, triggered by the retinal lesions, axonal arbors can change dramatically in a matter of hours. A second observation afforded by our ability to follow the same axon in vivo over multiple time points is the dynamic nature of the change, involving concurrent sprouting and pruning. The massive axonal turnover on a weekly basis resulted in a modest net increase in axonal density. It is likely, given previous results from much longer postlesion periods (Darian-Smith and Gilbert, 1994), that in the LPZ, axons continue to gradually increase in density. At 6 months to 1 year following the lesion, the density of horizontal axon collaterals in the LPZ has typically risen 2-fold relative to that of normal cortex (Darian-Smith and Gilbert, 1994).

It is informative to compare this efflorescence of axonal arbors with the time course of RF changes measured with electrophysiological recordings. The rapid change in the RFs of neurons just inside the LPZ (Gilbert and Wiesel, 1992), including shifts and RF expansion, parallels the short-term increase in axonal density seen here. The subsequent contraction of RFs matches the decrease in the density of axons in the LPZ over the subsequent weeks. The remapping of cortical topography, which progresses toward the center of the LPZ over long time periods, can be explained by a gradual build up of axon density in the LPZ.

Our data show that in response to retinal lesions, there is an initial exuberant outgrowth followed by a concomitant process of elimination. This is reminiscent of the transient overproduction of axons and synapses that occurs during development (Kasthuri and Lichtman, 2004; Niell et al., 2004). For example, geniculocortical arbors initially cover a large cortical territory during the first postnatal week and are then refined and coalesce to form the basis of ocular dominance columns (Ferster and LeVay, 1978; Levay and Stryker, 1979; LeVay et al., 1980). Intracortical connections show a similar process of refinement. The horizontal axon collaterals from pyramidal cells are initially fairly uniformly distributed at postnatal days 4 to 6 but are selectively pruned by postnatal days 28–35 with the remaining axons forming enriched clusters of collaterals (Callaway and Katz, 1990). Here, we observed both axonal retraction and degeneration, processes associated with development, (Low and Cheng, 2005, 2006; Luo and O'Leary, 2005; Portera-Cailliau et al., 2005). Taken together, the axonal restructuring that we observed in the adult appear to recapitulate programs seen in early development.

While the rapidity of the changes observed here was unexpected, there is precedence for such rapid change. Several studies show that axons during development have the capability to undergo dramatic changes. Axonal arborization increases by 50% over an 8 hr period in *Xenopus* tadpoles (Witte et al., 1996) and cortical axons in postnatal mouse can gain up to 35 μm/hr or lose up to 25 μm/hr (Portera-Cailliau et al., 2005). Experience causes rapid alterations in axonal arbors during critical periods in postnatal development. Monocular deprivation for 6–7 days induces a gain in complexity of thalamocortical arbors serving the nondeprived eye, while the ones corresponding to the deprived eye show a gross reduction (Antonini and Stryker, 1993). Furthermore, the induction of divergent strabismus in kittens for only 2 days produces a rapid withdrawal of horizontal connections from opposite-eye columns in layer 2/3 (Trachtenberg and Stryker, 2001).

The expectation that the adult cortex must have access to different cell-biological mechanisms than those existing early in development has already been challenged by the physiological findings on rapid remapping of cortical topography following retinal lesions. Furthermore, the background of a dynamic turnover of axonal boutons constitutes evidence that the cortex is, in a very real sense, primed for growth, and that the lack of input may trigger an increase in the level of synapse addition and elimination. Also, an analysis of signal transduction mechanisms underlying this process has shown upregulation of genes known to be involved in creating the axonal cytoskeleton (notably the Rho GTPase pathway) (Chen et al., 2009). That large-scale changes in axonal arbors occur following sensory deprivation has already been established in long-term studies (Darian-Smith and Gilbert, 1994; Florence et al., 1998; Kossut and Juliano, 1999). More rapid changes at the level of dendritic spines occur within days of retinal lesions in the mouse (Keck et al., 2008; also see Hickmott and Steen, 2005). Additionally, the continuous stimulation of a single whisker for 24 hr in freely moving adult mice causes a 36% increase of synaptic density (both excitatory and inhibitory) in the corresponding cortical barrel (Knott et al., 2002). Consequently, the evidence emerging from physiological, molecular and imaging studies, along with the current study,

converge to form a picture of a highly dynamic circuitry and functional architecture even in the adult cerebral cortex.

Axonal Dynamics in the Peri-LPZ

Large-scale branching patterns remain unchanged in the adult cortex during normal experience (De Paola et al., 2006; Stettler et al., 2006). In contrast, we found that following retinal lesions, axons are dynamic in the peri-LPZ. Although axon density was maintained, axonal turnover was similar to that inside the LPZ. This suggests that the peri-LPZ is different from normal cortex, i.e., the cortical state in the absence of a retinal lesion. In fact, retinal lesions cause changes in the expression of immediate early genes and neurotransmitter levels inside and outside of the LPZ (Chen et al., 2009; Hu et al., 2009; Massie et al., 2003a, 2003b). Moreover, previous studies (Gilbert and Wiesel, 1992) suggest that the RF shifts are not limited to the LPZ but extend outward into the peri-LPZ. This effectively maintains optimal sampling of the remaining retinal space, reflecting a process of decorrelation or maximal distancing of RF properties between neighboring neurons. The mechanism of this, at the level of circuitry, may be the destabilization of axon collaterals of peri-LPZ neurons that project both into the LPZ, which provides the signal that stimulates the process of axon turnover, and into the peri-LPZ. The difference observed between LPZ and peri-LPZ could be the newly available active postsynaptic sites in the LPZ, which are freed by the silencing of the direct interlaminar input and are taken over by the horizontal connections. This would lead to the observed net increase in the density of horizontal collaterals in the LPZ, but not the peri-LPZ, which retains active interlaminar input.

The dramatic increase in axonal bouton density among retained axons following a lesion indicates that sensory deprivation alters the normal dynamics of bouton turnover (~7% per week rate observed in normal cortex, De Paola et al., 2006 and Stettler et al., 2006). Instead of the rates of addition and elimination being balanced, more boutons are added initially than disappear. The initial axonal exuberance in the LPZ is paralleled by the increase in bouton density. At later time points, the densities of both axon collaterals and boutons return close to the values before the lesion, although the axonal density remains somewhat elevated. The increase in bouton turnover following alteration in visual experience complements findings in spine dynamics in vivo (Keck et al., 2008; Trachtenberg et al., 2002).

Our results demonstrate that the adult brain is capable of very rapid changes in circuitry following sensory deprivation and suggest that the fast remodeling of long-range horizontal connections accounts for the rapid functional reorganization of visual cortex observed from the onset of retinal lesions. These findings raise the possibility that similar circuit dynamic rewiring can occur under normal conditions and may underlie experience-dependent change in cortex, such as that associated with perceptual learning.

EXPERIMENTAL PROCEDURES

Animal Preparation and Viral Injections

All AAV-EGFP injections and two-photon imaging sessions were performed as described (Stettler et al., 2006) in two anesthetized adult primates (*Macaca fascicularis*) in accordance with institutional and federal guidelines for the treatment of animals.

Following initial induction of anesthesia with ketamine (10 mg/kg body weight), a venous cannula was inserted and the animal was intubated with an endotracheal tube. Anesthesia was maintained with pentobarbital (7 mg/kg/hr). The animal was placed in a stereotaxic apparatus. Heart rate and breathing were monitored throughout the experiment. Under sterile conditions, the scalp was retracted and a craniotomy of 5 mm × 15 mm was made overlying the V1/V2 border. The dura was opened and a high-titer preparation of AAV (100 nl containing 1.6×10^9 viral particles) was pressure injected into the cortex (several pulses at 0.1 bar for 1 min, with 3–5 min resting period afterward) through borosilicate glass micropipettes (World Precision Instruments, Inc.) using a Picospritzer III (Parker Hannifin Corp.). AAV-EGFP was injected in V1 at a depth of 500 μm to label neurons with somata in layer 2/3. The AAV-EGFP was made as previously described (Stettler et al., 2006). After viral injection, a small piece of artificial dura (Tecoflex, Thermedics, Inc.) was positioned atop the cortex, the dura was sutured, the excised piece of bone was reinserted and secured with surgical cyanoacrylate (Vetbond, 3M), and the scalp wound was closed. After the surgery, the animal was returned to its cage where it remained until imaging began. Since the AAV strain used is nonreplicative, only those neurons that were infected during the viral injections will express EGFP.

At the start of the first imaging session, the animal was fitted with a headpost. A craniotomy, ~16 mm in diameter, was made to expose the dura over the opercular surface, and a custom-designed stainless-steel chamber was affixed to the bone over the craniotomy with dental acrylic (Perm Reline & Repair Resin, Coltène Whaledent, Inc.). Since the Macaque dura is opaque, it was removed prior to the first imaging session, along with the artificial dura inserted at the time of injection. This preparation allows ~2 months of two-photon imaging before the cortex is covered with a membrane that is impenetrable to focused infrared light. While overgrowth can be removed in the initial weeks, it eventually becomes adherent to the cortex and cannot be removed without damaging the cortical vasculature. To maximize the time over which we could obtain images following the retinal lesion, we restricted ourselves to one imaging session before lesion placement.

Tissue regrowth was minimized by the use of two dura substitutes while the animal was not being imaged (Figure 1A, "resting"). A round flat artificial dura (EG-93A, Tecoflex Clear, Lubrizol Advanced Materials, Inc.) of 24 mm in diameter was placed on top of the cortex. A second premolded artificial dura (RTV615, Momentive Performance Materials, Inc.) placed on top of the first one, consisted of a round sheet of 23 mm in diameter, on top of which was a 13 mm external diameter ring, 1 mm thick and 7 mm high, which prevented the dura from growing into the center of the chamber (modified from Arieli et al., 2002). The chamber was then filled with 1.5% agarose (Type IIIA, Sigma Aldrich Co). During imaging sessions both artificial duras were replaced by a single one similar to the second artificial dura, but with the bottom consisting of only a 12 mm glass coverslip (Warner Instruments, LLC) (Figure 1A, "imaging session"). The interior of the chamber was cleaned at the start of each imaging session. This included the stripping of connective tissue covering the pia within the craniotomy.

In Vivo Imaging

Imaging was performed (largely as described in Stettler et al., 2006) using a custom-built microscope based on a Leica MP RS resonant microscope with a 40× water-immersion objective (Nikon FLUOR 40X/0.8W DIC M). Two-photon excitation (900–920 nm) was provided by a mode-locked Ti:sapphire laser pumped by a 10 W frequency-doubled Nd:Vanadate Laser (Tsunami/Millenia system, Spectra Physics). Imaging of EGFP used the following filter set: peak 525 nm, bandwidth 50 nm. Image acquisition was controlled by Leica Confocal Software (Leica, Germany). To minimize cerebral movement artifacts while imaging, we designed a system that phased-locked the acquisition of images with the animal breathing cycle.

During the first session, imaging began by locating the injection sites using the vascular pattern on the brain surface as fiduciary marks. Subsequently, nearby regions of cortex containing EGFP-labeled axons were identified and targeted for imaging on multiple occasions. To specifically image long-range longitudinal projections from EGFP-labeled pyramidal neurons in V1, these

regions were located 1.5-2 mm laterally and medially from the injection sites in V1. After each imaging session, the animal was put back in its cage to recover from the anesthesia.

Mapping Cortical RFs and Retinal Lesions

RFs were mapped as previously described (Darian-Smith and Gilbert, 1995). Briefly, a week after the initial imaging session, using insulated tungsten microelectrode (impedance 1–2 MΩ, Alpha Omega, Israel), evenly spaced penetrations were made perpendicular to the cortical surface and restricted to the superficial layers. Recordings were not made in the areas already imaged to avoid possible artifacts due to microelectrode penetrations. At each location, RFs were mapped according to "minimum response" characteristics using a hand-held stimulator, and properties such as orientation selectivity and ocular dominance were noted. To minimize eye movement, the animals were paralyzed during mapping with a paralytic agent (vecuronium bromide, induction 60 ml/hr, maintenance 6 ml/hr).

Retinal lesions were made as described previously (Gilbert et al., 1990; Gilbert and Wiesel, 1992). Briefly, the electrode was returned to a location inside the boundaries of the desired site of the lesion. The lesion was placed to include an area that was lateral from the injection sites, and that had already been imaged during the first imaging session. We localized the region of the retina corresponding to the recorded neuron using audio output from the electrode and a guide light from the ophthalmic laser (Iridex Corp.) as the visual stimulus. Visually driven activity from cortical neurons was thus used to guide the placement of the lesions. Once retinal lesions had been made in the appropriate locus, cortical cells within the LPZ immediately became unresponsive to visual stimulation. Alterations in the response properties from neurons outside the LPZ were immediately documented after retinal lesions had been made and again, to confirm the extent of the lesion, before the second imaging session. Typically, the diode laser delivered 300 mW for 800–1000 ms.

Image Analysis

Axons were identified and traced by hand, with the aid of Neuromantic software (www.rdg.ac.uk/neuromantic/), in Z stacks that had been processed with a median filter to reduce noise (ImageJ, rsb.info.nih.gov/ij/). The semiautomated tracing of axons involved the examination in multiple viewings of Z stacks at different brightness and contrast levels as well as different zoom levels. Despite the use of the artificial dura and synchronizing the acquisition with the breathing cycle, brain movement on the order of one to a few micrometers in all three dimensions sometimes occurred. Therefore, we wrote an alignment program in Matlab (The MathWorks, Inc.) that translates each image in a 3D stack so that the cortical volume is reconstructed as accurately as possible. The program is constrained so that only translations of each image in the X, Y, or Z directions are allowed (rotations and image warping are prohibited). First, the program automatically aligns all the images in a stack in the X-Y plane; second, it rearranges the images in the Z direction to ensure that adjacent images in the realigned stack correspond to adjacent cortical depths. The first step uses steepest descent minimization to find the lateral alignment of each image that minimizes the appearance of 'duplicated' axons and cell bodies in the maximum value Z projection of the stack. The second step shuffles the realigned image slices to find the appropriate depth for each image that maximizes the similarity of adjacent slices over the whole stack. Importantly, the program features a graphical user interface that allows the user to manually and interactively modify the results from the automatic X-Y and Z alignments. The user intervention reduces the susceptibility of the program to local minima and ensures that the alignments are appropriate.

Bootstrapping Statistics

We used a bootstrapping procedure (Efron and Tibshirani, 1994) to test the null hypothesis that the increase in axonal density between two time points in MA or MB was a stochastic fluctuation. We grouped all the axons that were present at either of the two time points, and formed a sample distribution $\hat{D}$, which expresses the difference in length for each axon between the two time points. Let $L_{i,j}$ be the length of the i-th axon at time point j (where j = 1 or 2); then $\hat{D} = \{L_{1,2} - L_{1,1}, L_{2,2} - L_{2,1}, L_{3,2} - L_{3,1}, \ldots, L_{N,2} - L_{N,1}\}$, where N is the total number of unique axons present at either time point. (Axons that were absent at one time point or another are assumed to have length 0.) We used the bootstrapping procedure, which resamples the distribution $\hat{D}$ with replacement, to compute the probability distribution for the mean change in axonal length between the two time points. The p value is the probability that the mean change in axonal length among any random resampling from $\hat{D}$ is less than or equal to 0 μm (we used 100,000 bootstrapping iterations).

Statistical Comparisons between the Control and the LPZ

Brunner-Munzel Test

We compared the distribution of axonal changes seen in the control study (Stettler et al., 2006) to the distribution obtained from the LPZ using the Brunner-Munzel test (Brunner and Munzel, 2000). This is a nonparametric procedure used to test the null hypothesis that the medians of two sample distributions are equivalent. (The Brunner-Munzel test makes no assumptions whatsoever about the shapes of the two distributions under comparison, so it is more general than other non-parametric alternatives to the t test, like the Wilcoxon rank-sum test.)

In order to obtain the control and LPZ distributions, we measured the percent change in axonal length, from the first to the second time point, for each axon in the control and experimental data sets, using custom Matlab software (The MathWorks, Inc.) Let $C_{i,j}$ be the length of the i-th axon, at the j-th time point, from the control data; likewise, let $L_{m,n}$ be the length of axon m at time point n, in the LPZ. Then ΔC_i and ΔL_m, the percentage change in the length of these axons, were calculated according to the equations:

$$\Delta C_i = (C_{i,2} - C_{i,1})/C_{i,1} \times 100\%$$

$$\Delta L_m = (L_{m,2} - L_{m,1})/L_{m,1} \times 100\%$$

for $1 \leq i \leq 84$ and $1 \leq m \leq 159$ (there were 84 axons in the sample from the control data and 159 from the current study). The sample distributions of axonal changes from the control and lesion cortices were $\hat{D}_1$ and $\hat{D}_2$, respectively:

$$\hat{D}_1 = \{\Delta C_1, \Delta C_2, \Delta C_3, \ldots, \Delta C_{84}\}$$

$$\hat{D}_2 = \{\Delta L_1, \Delta L_2, \Delta L_3, \ldots, \Delta L_{159}\}$$

Whenever any axon was present at one time point, but absent at the other, its length at the "absent" time point was taken to be 1 μm (i.e., the axon was modeled as a "point" rather than as a nonexisting segment; we applied this minor adjustment to avoid dividing by zero in the formulae listed above). After extracting them from the data, the two distributions ($\hat{D}_1$ and $\hat{D}_2$) were compared with a one-sided Brunner- Munzel test, to verify that the difference between them was unlikely to result from chance.

Resampling Test

As an alternative to the Brunner-Munzel procedure, we performed a statistical resampling test, in order to explicitly demonstrate that the lack of axonal dynamics in the control study (Stettler et al., 2006) was not the result of limited axonal sampling. There were 84 axons in the sample we reanalyzed from the control data. So at each iteration of the resampling procedure, we randomly sampled a subset of 84 axons from the LPZ, with replacement (there were 159 axons in the LPZ sample). For each randomly selected subset of axons from the LPZ, we measured the total axonal length at both time points, and then calculated the percent change in total axonal length, from the first to the second time point. (Here, since we were considering the total axonal length over a population of axons, rather than the length of individual axons, we did not substitute "point" axons for axonal segments that were absent at one time point or another.) We repeated this procedure for 100 million iterations, and computed the p value as the fraction of iterations for which the axonal sprouting in the sampled subset was less than or equal to the sprouting seen in the control study.

ACKNOWLEDGMENTS

This work was supported by NIH grant EY018119. The authors would like to thank Matthew Isakson for technical assistance.

Accepted: October 30, 2009
Published: December 9, 2009

REFERENCES

Antonini, A., and Stryker, M.P. (1993). Rapid remodeling of axonal arbors in the visual cortex. Science *260*, 1819–1821.

Arieli, A., Grinvald, A., and Slovin, H. (2002). Dural substitute for long-term imaging of cortical activity in behaving monkeys and its clinical implications. J. Neurosci. Methods *114*, 119–133.

Baker, C.I., Peli, E., Knouf, N., and Kanwisher, N.G. (2005). Reorganization of visual processing in macular degeneration. J. Neurosci. *25*, 614–618.

Brunner, E., and Munzel, U. (2000). The nonparametric Behrens-Fisher problem: Asymptotic theory and a small sample approximation. Biom. J. *42*, 17–25.

Calford, M.B., Wang, C., Taglianetti, V., Waleszczyk, W.J., Burke, W., and Dreher, B. (2000). Plasticity in adult cat visual cortex (area 17) following circumscribed monocular lesions of all retinal layers. J. Physiol. *524*, 587–602.

Calford, M.B., Chino, Y.M., Das, A., Eysel, U.T., Gilbert, C.D., Heinen, S.J., Kaas, J.H., and Ullman, S. (2005). Neuroscience: rewiring the adult brain. Nature *438*, E3.

Callaway, E.M., and Katz, L.C. (1990). Emergence and refinement of clustered horizontal connections in cat striate cortex. J. Neurosci. *10*, 1134–1153.

Chen, J., Yamahachi, H., and Gilbert, C.D. (2009). Experience-dependent gene expression in adult visual cortex. Cereb. Cortex, in press. Published online July 1, 2009. 10.1093/cercor/bhp131.

Chino, Y.M., Kaas, J.H., Smith, E.L., 3rd, Langston, A.L., and Cheng, H. (1992). Rapid reorganization of cortical maps in adult cats following restricted deafferentation in retina. Vision Res. *32*, 789–796.

Chino, Y.M., Smith, E.L., 3rd, Kaas, J.H., Sasaki, Y., and Cheng, H. (1995). Receptive-field properties of deafferentated visual cortical neurons after topographic map reorganization in adult cats. J. Neurosci. *15*, 2417–2433.

Crist, R.E., Li, W., and Gilbert, C.D. (2001). Learning to see: experience and attention in primary visual cortex. Nat. Neurosci. *4*, 519–525.

Darian-Smith, C., and Gilbert, C.D. (1994). Axonal sprouting accompanies functional reorganization in adult cat striate cortex. Nature *368*, 737–740.

Darian-Smith, C., and Gilbert, C.D. (1995). Topographic reorganization in the striate cortex of the adult cat and monkey is cortically mediated. J. Neurosci. *15*, 1631–1647.

Das, A., and Gilbert, C.D. (1995). Long-range horizontal connections and their role in cortical reorganization revealed by optical recording of cat primary visual cortex. Nature *375*, 780–784.

De Paola, V., Holtmaat, A., Knott, G., Song, S., Wilbrecht, L., Caroni, P., and Svoboda, K. (2006). Cell type-specific structural plasticity of axonal branches and boutons in the adult neocortex. Neuron *49*, 861–875.

Denk, W., Strickler, J.H., and Webb, W.W. (1990). Two-photon laser scanning fluorescence microscopy. Science *248*, 73–76.

Efron, B., and Tibshirani, R.J. (1994). An Introduction to the Bootstrap (New York: Chapman & Hall).

Ferster, D., and LeVay, S. (1978). The axonal arborizations of lateral geniculate neurons in the striate cortex of the cat. J. Comp. Neurol. *182*, 923–944.

Florence, S.L., Taub, H.B., and Kaas, J.H. (1998). Large-scale sprouting of cortical connections after peripheral injury in adult macaque monkeys. Science *282*, 1117–1121.

Giannikopoulos, D.V., and Eysel, U.T. (2006). Dynamics and specificity of cortical map reorganization after retinal lesions. Proc. Natl. Acad. Sci. USA *103*, 10805–10810.

Gilbert, C.D., and Wiesel, T.N. (1979). Morphology and intracortical projections of functionally characterised neurones in the cat visual cortex. Nature *280*, 120–125.

Gilbert, C.D., and Wiesel, T.N. (1992). Receptive field dynamics in adult primary visual cortex. Nature *356*, 150–152.

Gilbert, C.D., Hirsch, J.A., and Wiesel, T.N. (1990). Lateral interactions in visual cortex. Cold Spring Harb. Symp. Quant. Biol. *55*, 663–677.

Heinen, S.J., and Skavenski, A.A. (1991). Recovery of visual responses in foveal V1 neurons following bilateral foveal lesions in adult monkey. Exp. Brain Res. *83*, 670–674.

Hickmott, P.W., and Steen, P.A. (2005). Large-scale changes in dendritic structure during reorganization of adult somatosensory cortex. Nat. Neurosci. *8*, 140–142.

Hirsch, J.A., and Gilbert, C.D. (1991). Synaptic physiology of horizontal connections in the cat's visual cortex. J. Neurosci. *11*, 1800–1809.

Hu, T.T., Laeremans, A., Eysel, U.T., Cnops, L., and Arckens, L. (2009). Analysis of c-fos and zif268 expression reveals time-dependent changes in activity inside and outside the lesion projection zone in adult cat area 17 after retinal lesions. Cereb. Cortex *19*, 2982–2992.

Kaas, J.H., Krubitzer, L.A., Chino, Y.M., Langston, A.L., Polley, E.H., and Blair, N. (1990). Reorganization of retinotopic cortical maps in adult mammals after lesions of the retina. Science *248*, 229–231.

Kasthuri, N., and Lichtman, J.W. (2004). Structural dynamics of synapses in living animals. Curr. Opin. Neurobiol. *14*, 105–111.

Keck, T., Mrsic-Flogel, T.D., Vaz Afonso, M., Eysel, U.T., Bonhoeffer, T., and Hübener, M. (2008). Massive restructuring of neuronal circuits during functional reorganization of adult visual cortex. Nat. Neurosci. *11*, 1162–1167.

Knott, G.W., Quairiaux, C., Genoud, C., and Welker, E. (2002). Formation of dendritic spines with GABAergic synapses induced by whisker stimulation in adult mice. Neuron *34*, 265–273.

Kossut, M., and Juliano, S.L. (1999). Anatomical correlates of representational map reorganization induced by partial vibrissectomy in the barrel cortex of adult mice. Neuroscience *92*, 807–817.

Levay, S., and Stryker, M.P. (1979). The development of ocular dominance columns in the cat. Soc. Neurosci. Symp. *4*.

LeVay, S., Wiesel, T.N., and Hubel, D.H. (1980). The development of ocular dominance columns in normal and visually deprived monkeys. J. Comp. Neurol. *191*, 1–51.

Li, W., Piëch, V., and Gilbert, C.D. (2004). Perceptual learning and top-down influences in primary visual cortex. Nat. Neurosci. *7*, 651–657.

Li, W., Piëch, V., and Gilbert, C.D. (2006). Contour saliency in primary visual cortex. Neuron *50*, 951–962.

Low, L.K., and Cheng, H.J. (2005). A little nip and tuck: axon refinement during development and axonal injury. Curr. Opin. Neurobiol. *15*, 549–556.

Low, L.K., and Cheng, H.J. (2006). Axon pruning: an essential step underlying the developmental plasticity of neuronal connections. Philos. Trans. R. Soc. Lond. B Biol. Sci. *361*, 1531–1544.

Luo, L., and O'Leary, D.D. (2005). Axon retraction and degeneration in development and disease. Annu. Rev. Neurosci. *28*, 127–156.

Majewska, A.K., Newton, J.R., and Sur, M. (2006). Remodeling of synaptic structure in sensory cortical areas *in vivo*. J. Neurosci. *26*, 3021–3029.

Massie, A., Cnops, L., Jacobs, S., Van Damme, K., Vandenbussche, E., Eysel, U.T., Vandesande, F., and Arckens, L. (2003a). Glutamate levels and transport in cat (Felis catus) area 17 during cortical reorganization following binocular retinal lesions. J. Neurochem. *84*, 1387–1397.

Massie, A., Cnops, L., Smolders, I., Van Damme, K., Vandenbussche, E., Vandesande, F., Eysel, U.T., and Arckens, L. (2003b). Extracellular GABA concentrations in area 17 of cat visual cortex during topographic map reorganization following binocular central retinal lesioning. Brain Res. *976*, 100–108.

Mataga, N., Mizuguchi, Y., and Hensch, T.K. (2004). Experience-dependent pruning of dendritic spines in visual cortex by tissue plasminogen activator. Neuron *44*, 1031–1041.

McManus, J.N., Ullman, S., and Gilbert, C.D. (2008). A computational model of perceptual fill-in following retinal degeneration. J. Neurophysiol. *99*, 2086–2100.

Niell, C.M., Meyer, M.P., and Smith, S.J. (2004). *In vivo* imaging of synapse formation on a growing dendritic arbor. Nat. Neurosci. *7*, 254–260.

Palagina, G., Eysel, U.T., and Jancke, D. (2009). Strengthening of lateral activation in adult rat visual cortex after retinal lesions captured with voltage-sensitive dye imaging in vivo. Proc. Natl. Acad. Sci. USA *106*, 8743–8747.

Portera-Cailliau, C., Weimer, R.M., De Paola, V., Caroni, P., and Svoboda, K. (2005). Diverse modes of axon elaboration in the developing neocortex. PLoS Biol. *3*, e272.

Reimsnider, S., Manfredsson, F.P., Muzyczka, N., and Mandel, R.J. (2007). Time course of transgene expression after intrastriatal pseudotyped rAAV2/1, rAAV2/2, rAAV2/5, and rAAV2/8 transduction in the rat. Mol. Ther. *15*, 1504–1511.

Rose, J.E., Malis, L.I., Kruger, L., and Baker, C.P. (1960). Effects of heavy, ionizing, monoenergetic particles on the cerebral cortex. II. Histological appearance of laminar lesions and growth of nerve fibers after laminar destructions. J. Comp. Neurol. *115*, 243–255.

Ruthazer, E.S., Li, J., and Cline, H.T. (2006). Stabilization of axon branch dynamics by synaptic maturation. J. Neurosci. *26*, 3594–3603.

Schoups, A., Vogels, R., Qian, N., and Orban, G. (2001). Practising orientation identification improves orientation coding in V1 neurons. Nature *412*, 549–553.

Smirnakis, S.M., Brewer, A.A., Schmid, M.C., Tolias, A.S., Schüz, A., Augath, M., Inhoffen, W., Wandell, B.A., and Logothetis, N.K. (2005). Lack of long-term cortical reorganization after macaque retinal lesions. Nature *435*, 300–307.

Stettler, D.D., Das, A., Bennett, J., and Gilbert, C.D. (2002). Lateral connectivity and contextual interactions in macaque primary visual cortex. Neuron *36*, 739–750.

Stettler, D.D., Yamahachi, H., Li, W., Denk, W., and Gilbert, C.D. (2006). Axons and synaptic boutons are highly dynamic in adult visual cortex. Neuron *49*, 877–887.

Trachtenberg, J.T., and Stryker, M.P. (2001). Rapid anatomical plasticity of horizontal connections in the developing visual cortex. J. Neurosci. *21*, 3476–3482.

Trachtenberg, J.T., Chen, B.E., Knott, G.W., Feng, G., Sanes, J.R., Welker, E., and Svoboda, K. (2002). Long-term *in vivo* imaging of experience-dependent synaptic plasticity in adult cortex. Nature *420*, 788–794.

Witte, S., Stier, H., and Cline, H.T. (1996). *In vivo* observations of timecourse and distribution of morphological dynamics in Xenopus retinotectal axon arbors. J. Neurobiol. *31*, 219–234.